IEEE Access
The journal for rapid open access publishing

SPECIAL SECTION ON TOWARD UBIQUITOUS REAL-TIME RADIO PROPAGATION MODELING: THE EXPLOITATION OF CYBER RESOURCES, GPU AND FAST AND ACCURATE EM ALGORITHMS

Received November 2, 2015, accepted November 30, 2015, date of publication December 18, 2015, date of current version January 6, 2016.

Digital Object Identifier 10.1109/ACCESS.2015.2510363

Dynamic Channel Modeling for an Indoor Scenario at 23.5 GHz

NAN ZHANG[1], JIANWU DOU[1], LI TIAN[1], XI YUAN[1], XIAOYI YANG[1], SUPING MEI[1], AND HAIMING WANG[2]

[1]Wireless Algorithm Department, Product Research and Development System, ZTE Corporation, Shanghai 201203, China
[2]State Key Laboratory of Millimeter Waves, Southeast University, Nanjing 211111, China

Corresponding author: N. Zhang (zhang.nan152@zte.com.cn)

This work was supported in part by the National Science and Technology Major Project of China under Grant 2014ZX03003010 and in part by the 973 Program of China under Grant 2013CB329002.

ABSTRACT In this paper, the dynamic channel characteristics at 23.5 GHz in an indoor scenario are investigated according to measurement and deterministic simulation. In order to obtain accurate channel realizations, the ray tracing (RT) software is calibrated on both the power delay profile and the path levels. For the measurement data, the propagation paths are identified using the non-parametric peak detection algorithm. The cluster-alike behaviors of these paths and the influence of the antenna radiation pattern are also studied through the comparison with the RT simulated paths. Subsequently, the evolutionary traces of channel with regard to the user equipment's movement are identified by associating the samples, which have the similar parameters at adjacent locations. The features of these traces are analyzed in both statistical and individual ways. Results show that the life durations of most traces are within 5 m. The line of sight and reflected paths with significant power survive longer than the others. These observations confirm the feasibility of designing adaptive beam tracking algorithms based on the spatial consistency of the dominant propagation paths. Moreover, high correlations among the variations of different parameters in the same trace are revealed.

INDEX TERMS 23.5 GHz, dynamic channel modeling, life duration of trace, spatial consistency, beam tracking.

I. INTRODUCTION

With the initialization of the fifth generation mobile communication system (5G), several techniques, i.e., massive multiple-input and multiple-output (MIMO), beamforming and millimeter wave communications are considered as the promising candidates to achieve the 1000× capacity growth comparing with the LTE-Advanced system [1]–[5]. For designing the mobile communication systems and evaluating their performance, it has became pivotal to establish the accurate channel models.

Recently the channel measurement campaigns, which were conducted by adopting the channel sounding system equipped with high-directivity antennas, became popular for channel studying at high frequencies. Many results based on these kinds of measurements have been published, as shown in [2] and [6]–[8]. However, since the narrow-beam antennas need to be rotated over all the azimuth-elevation pairs to capture the complete channel spatial characteristics, the time consumption of the measurement drastically increases. Sufficiently accurate channel samples are difficult to be collected for studying the variations of channel with regard to the change of time or UE's location. Consequently, these literatures mainly focus on investigating the static channel properties, such as the large-scale and cluster-level parameters. Since the channel evolutionary properties, i.e., the spatial consistency and time-variation, are not involved, these results are not sufficient to evaluate the performance of some new 5G techniques, i.e., massive-MIMO and beam tracking [9].

Current researches show that the propagation channel at high frequencies can be accurately reproduced by involving the combination of several paths originating from LoS, specular reflection, diffraction or background scattering due to the much severe propagation and penetration loss [10]–[12]. It has been found that the ray-based deterministic modeling approaches with low complexity are suitable for studying the high-frequency channels since they are flexible to be implemented in various cases under

FIGURE 1. The panorama of the indoor measurement environment.

different configurations. Besides, the channel evolutionary behaviors over time and spatial domains can be easily and accurately represented in the deterministic way. In this paper, for well-describing the dynamic properties of channel,[1] the propagation channel is investigated by conducting extensive measurements with the pre-configured UE's trajectory. Meanwhile, the RT simulations with the same configurations are also adopted to assist the channel analysis.

The rest of the paper is organized as follows. In Section II, the data acquisitions based on measurement and ray-tracing are introduced briefly. Section III elaborates the data post-processing procedures and the comparison between the measurement and simulation results. The individual analysis of identified traces and the statistical modeling of the dynamic channel features are presented in section IV. Finally, conclusive remarks are given in Section V.

II. DATA ACQUISITION

A. MEASUREMENT CAMPAIGN

The panorama of the environment is depicted in figure 1, which is a typical indoor conference scenario with the geometric size equaling to $12 \times 9 \times 3$ m^3. The transmitter (Tx) was highly fixed at a corner of room to emulate an access point (AP) during the whole measurement. Totally 30 Rxs within the UE's movement trajectory shown in figure 2, were investigated. For each Rx, the channel frequency responses have been recorded by the VNA-based automatic channel sounding system [13]. An Agilent signal generator E8257D and an Agilent VNA N5245A in frequency-sweep mode were adopted at Tx and Rx, respectively. Both of them were synchronized by the common reference source. The measurement procedures and data storage were controlled by a laptop. Two vertical-polarized horn antennas were mounted on the customer-made rotary tables at both Tx and Rx. The spatial characteristics of propagation channel were captured by rotating the Tx and Rx antennas in both azimuth and elevation domains successively. The measurement configurations are listed in Table 1 and more details about the measurement can be found in [13] and [14].

[1]The dynamic properties of channel refer to the channel evolutionary behaviour over the time and location, i.e., spatial consistency, non-stationary and correlation between different UEs.

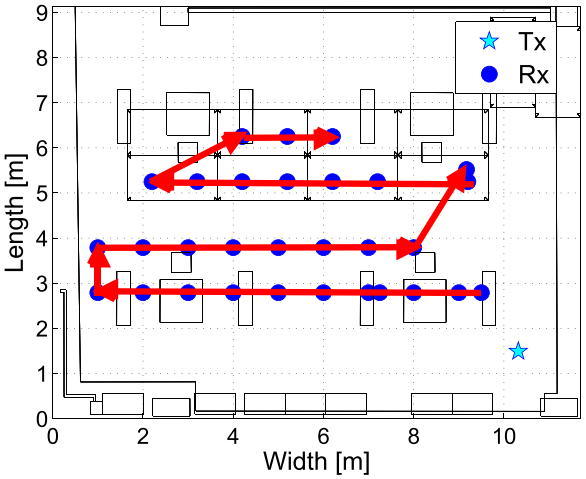

FIGURE 2. The movement trajectory of UE.

TABLE 1. The configurations of measurement.

Parameter	Settings
Center frequency	23.5 GHz
Bandwidth	660 MHz
Transmit Power	10 dBm
Antenna type	Linearly-polarized horn antenna
Antenna gain	18.9 dBi
Half-power beam width	18.2°
Frequency-Sweep points	256
Frequency-Sweep duration	80 ms
Cycles per Measurement	8
Tx hight	1.95 m
Rx hight	1 m
Tx Rotations	Elevation : -10° and -25° Azimuth : $-15^\circ : 15^\circ : -105^\circ$
Rx Rotations	Elevation : 0° and 15° Azimuth : $-165^\circ : 15^\circ : 180^\circ$

B. RAY-TRACING SIMULATION

A self-developed full 3D ray-tracing (RT) software was implemented in this research. Three main steps are introduced to generate the channel realizations in the specified scenario, i.e., constructing the detailed 3D digital map, calculating the geometric parameters for each propagation path and implementing the electromagnetic calculations according to propagation mechanisms, such as LoS, reflection and diffraction [15]–[17]. Meanwhile, the non-negligible diffuse scattering, which models the back-reflection from rough surfaces or non-homogenous materials, is also consid-

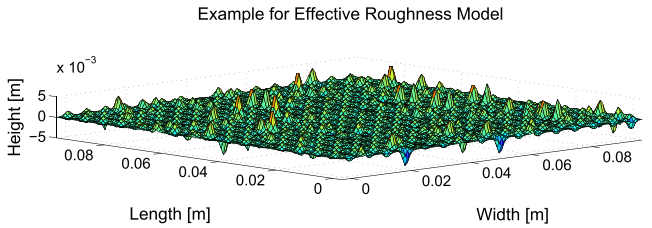

FIGURE 3. Illustration of the "effective roughness" scattering model.

ered in our RT platform [18]–[20]. To achieve it, the rough surfaces are firstly discretized into multiple small tiles as shown in figure 3. The far-field assumption should also be satisfied for each tile. Then a directive scattering pattern is adopted to calculate the amplitude of the scattering coefficients based on the ''effective roughness'' (ER) scattering model [21]. The phase of each scattering path is randomly assigned under the uncorrelated diffuse scattering assumption.

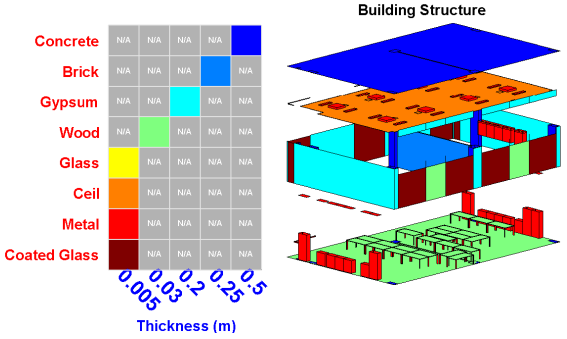

FIGURE 4. Digitized map for the specified scenario.

Figure 4 depicts the digitalized map of the measurement scenario. Different kinds of materials are color-coded according to the legend. The corresponding electromagnetic properties (i.e., relative permittivity and conductivity) at specified frequency are adopted depending on the ITU deliverable [22]. The verifications of the RT method are well done by comparing the simulated channel with the measurement results on both PDP and path-levels for all the UE's locations. More details about the calibrations can be found in [14] and [23]. Considering the trade-off between modeling accuracy and complexity, at most three reflections, one diffraction and one diffuse scattering together with ten penetrations are implemented in our simulations. The other configurations of RT, such as transmit power and antenna radiation patterns, are the same as the measurement for extensive simulations.

III. DATA ANALYSIS

For the further analysis of the small-scale channel characteristics, the measurement-based PDPs are firstly derived from the captured channel frequency responses as

$$P(\tau) = |h(\tau)|^2, \tag{1}$$

and

$$h(\tau) = \mathscr{F}^{-1}[H(f)], \tag{2}$$

where $H(f)$ is the channel transfer function in the frequency domain. $h(\tau)$ means the channel impulse response (CIR), and $\mathscr{F}^{-1}$ denotes the inverse Fourier transformation. Then the peak detection algorithm is adopted to identify the paths in delay domain [24], [25]. The spatial parameters[2] of these paths are assigned corresponding to the antenna rotated pairs, thus the spatial resolution is limited by the measurement configurations.

In order to get well understandings of the path's behaviors at high frequency and the influence of the antenna radiation pattern adopted in measurement, two kinds of RT simulations denoted as RT-1 and RT-2 have been conducted to emulate the measurement. The difference between these two simulations is: the spatial parameters of each path are directly calculated in RT-1, while the values of these angles for simulated paths in RT-2 are associated with direction pairs of the rotated Tx-Rx antenna, which emulates the same procedures implemented in the measurement.

An example of the obtained multi-paths from both RTs and measurement within the 30 dB dynamic range are shown in figure 5. The marker size represents the power of the path. By comparing the results, it is obvious that much more paths are detected from measurement instead of some sparsely distributed paths in RT-1 simulation, and the distribution of measurement-based paths is more cluster-alike. We assume that these differences are caused by the ''frosted glass'' phenomenon, which represents that the actual channel is ''blurred'' by the antenna pattern adopted in the current channel sounding system as demonstrated in figure 6. More specifically, the contribution of one physical path, i.e., $\delta(\Omega_{AoA})$ with the azimuth of arrival equalling to Ω_{AoA}, is captured several times since the radiation pattern of the rotated antenna is overlapped during the measurement. The received power of Rx in the ith rotated direction of antenna can be calculated as

$$p_i = |\delta(\Omega_{AoA}) * C(\Omega - (i-1)\cdot\Delta\Omega_{AoA})|^2, \quad i = 1:I, \tag{3}$$

where $*$ and $\cdot$ represent the convolutional and multiply operator, respectively. $C(\cdot)$ stands for the antenna pattern. I refers to the number of rotation and $\Delta\Omega_{AoA}$ is the rotation step of the Rx antenna in azimuth domain. Then, by adopting the non-parametric post-processing method for measurement data, some phantom paths, i,e., $p_i \cdot \delta(\Omega_{AoA} - (i-1)\cdot\Delta\Omega_{AoA})$, will be detected if the p_i is within the dynamic range. By further investigation, our proposed postulation is verified by the simulation results in RT-2. We can find that the paths in RT-2 match well with the detected results from measurement and the cluster-alike phenomenon is also reproduced as shown in figure 5.

[2]For certain path, the spatial parameters refer to the azimuth of arrival (AoA), elevation of arrival (EoA), azimuth of departure (AoD) and elevation of departure (EoD).

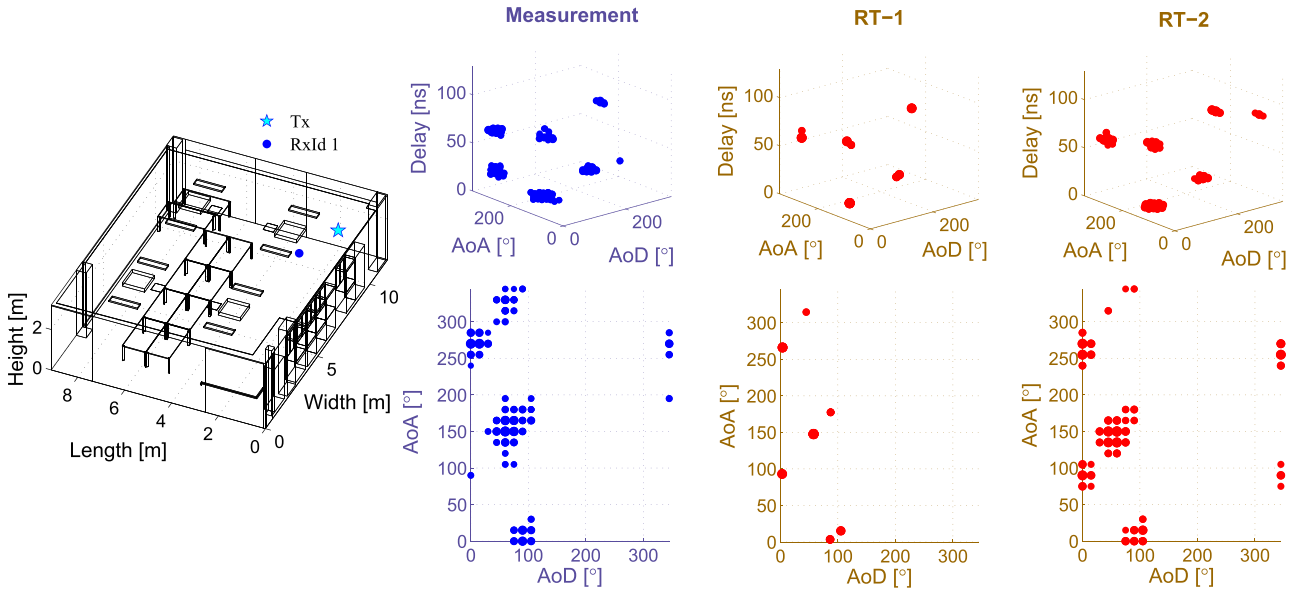

FIGURE 5. Comparison of the channel based on the measurement and RT simulations at No.1 Rx.

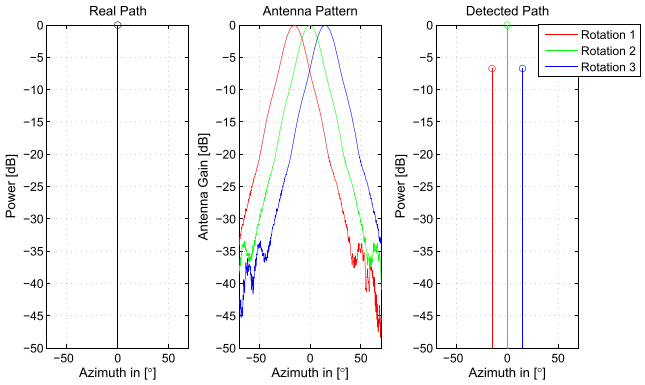

FIGURE 6. The schematic diagram of the "frosted glass" phenomenon.

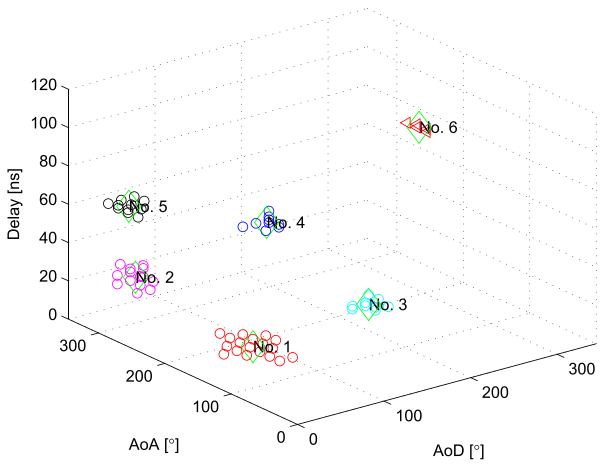

FIGURE 7. Clustering results using measurement data.

The K-power method is utilized for clustering of detected multi-path components (MPCs) obtained from the measurement as shown in figure 7 [26]. These centroids of clusters and simulated paths in RT-1 are used to identify the trace[3] along the UE's trajectory individually according to the following procedures:

1) Preparing the channel samples Θ_n for the nth measurement position along the UE's movement. Here, $\Theta_n = [\theta_n^l, \ldots, \theta_n^{L_n}], n = 1 : N$. All of the obtained parameters of lth centroid or path, i.e., power, delay and spatial parameters, are listed in $\theta_n^{L_n}$. The number of UE's locations and centroids or paths obtained in the nth measurement position are denoted as N and L_n, respectively.
2) Selecting the sample θ_n^l with the highest power as the start of the jth trace denoted as $\theta_j^{current}$. The n and j start from 1 for initialization.
3) Identifying the θ_j^{next} which satisfies

$$\begin{cases} \theta_j^{next} = \arg\min_l \{|\theta_m^l - \theta_j^{current}|\} \\ |\theta_j^{next} - \theta_j^{current}| \le T_\theta, \end{cases} \tag{4}$$

where the T_θ contains the empirical thresholds of different parameters and $m = n + 1$.
4) If the θ_j^{next} is selected and $m < N$, the process continues by re-starting step 3 with $\theta_j^{current} = \theta_j^{next}$ and $m = m + 1$. Otherwise, the searching for this trace is ended. The identification for the $j + 1$th starts from the step 2.
5) If all of the samples in θ_n^l are selected, the procedure will return to step 2 with $n = n + 1$. The whole process will be ended if $n > N$.

Totally 39 traces are observed from both measurement-based and simulated channels. All of the results are shown

[3]The trace refers to the continuously evolutionary behavior of the one path or cluster with regard to the change of time or UE's location. Similar phenomenon denoted as "time-evolving clusters" is described in [26] and [27].

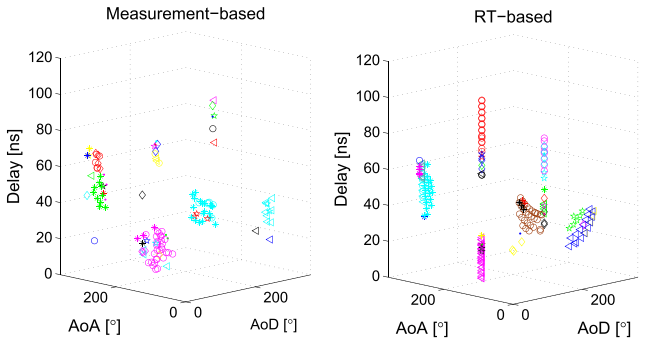

FIGURE 8. The results of trace association for both measurement and RT.

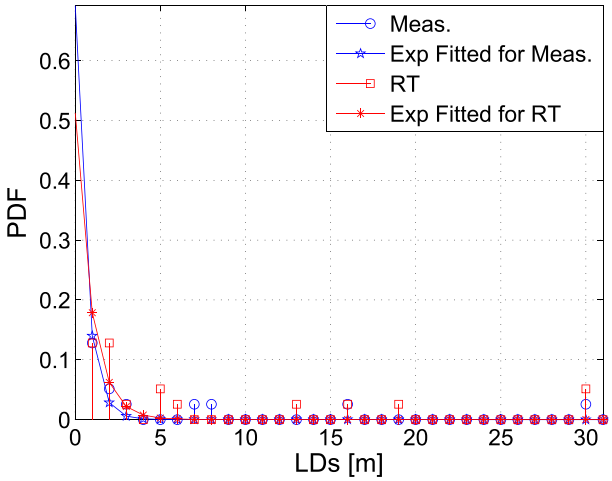

FIGURE 9. The PDFs of LDs for all traces obtained from both measurement and RT simulation.

in figure 8, in which the points with the same color and marker belong to same trace.

IV. MODELLING RESULTS

A. THE ANALYSIS OF ALL THE TRACES

For establishing the dynamic channel model, the statistical characteristics of the aforementioned traces are analyzed. As an important metric to evaluate the birth-death feature of the channel, the life duration (LD) of the jth trace is calculated as

$$LD_j = \sum_{n=n_j^1}^{n=n_j^2-1} |S_n - S_{n+1}|^2, \tag{5}$$

where n_j^1 and n_j^2 depict the indexes of the first and last locations in the jth trace. $S_n = [x_n\ y_n\ z_n]$ stands for the coordinate of nth measurement location. The probability distribution functions (PDFs) for the LDs of all the identified traces are depicted in figure 9. We can find that the LDs of 59% and 44% traces equal to zero for measurement-based and RT simulated results, respectively. It means that these channel components only can be observed at single location. We also find that the LDs are within 5 m for 90% measurement-based and 80% RT simulated traces. However, the LDs of the dominated paths with larger power are much longer. More specifically, one (LoS) and two (LoS + single bounce reflection) traces are observed at all UE's locations from measurement-based and RT simulated results, respectively. The distributions of LDs obtained from both measurement and RT simulation can be fitted by the exponential decay line with the decaying factor (λ) equalling to 1.60 and 1.05, respectively. It depicts that the LDs of RT-based traces are generally longer than those of the measurement results.

Additionally, the parameters variations of the jth trace between the nth and mth UE's locations are investigated by calculating their absolute values as

$$\Delta\theta_j^{n,m} = |\theta_j^n - \theta_j^m|, \quad (m, n) \in [n_j^1\ n_j^2]. \tag{6}$$

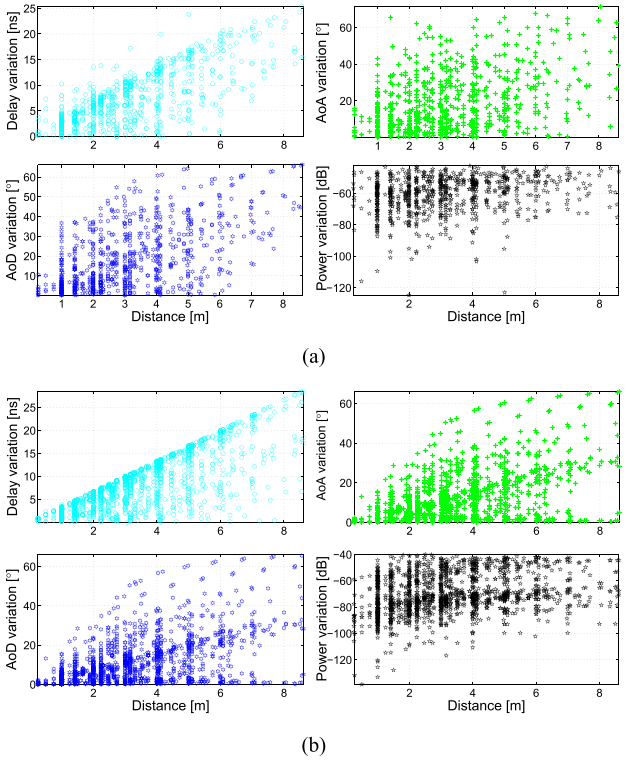

FIGURE 10. The analysis of parameters variations for both measurement and RT results. (a) Measurement-based. (b) RT-based.

TABLE 2. The cross-correlation coefficient between the variations of parameters for measurement-based trace.

Para	Delay	AoA	AoD	Power
Delay	1	0.29	0.15	0.25
AoA	0.29	1	0.38	0.24
AoD	0.15	0.38	1	0.19
Power	0.25	0.24	0.19	1

The relationship between $\Delta\theta_j^{n,m}$ and the corresponding distance of UE's movement, which is derived as $d_j^{n,m} = |S_n - S_m|^2$, is investigated. All of the results are shown in Figure 10. It can be found that the ranges of variations for these parameters are enlarged with the increasing of the distance between two UE's locations within the same trace. The

IEEE Access
The journal for rapid open access publishing

TABLE 3. The cross-correlation coefficient between the variations of parameters for RT-based trace.

Para	Delay	AoA	AoD	Power
Delay	1	0.08	0.08	0.35
AoA	0.08	1	0.99	0.40
AoD	0.08	0.99	1	0.40
Power	0.35	0.40	0.40	1

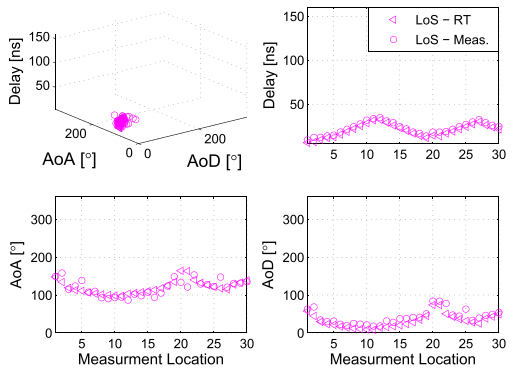

(a)

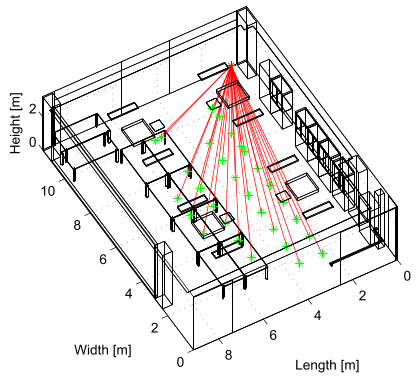

(b)

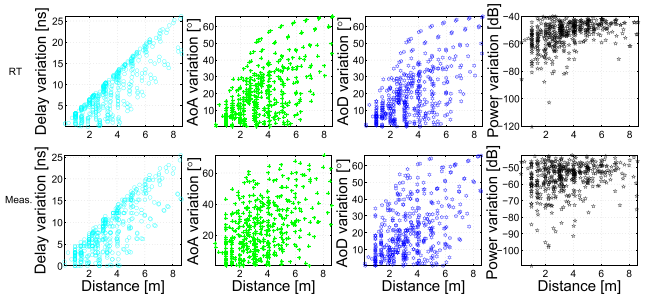

(c)

FIGURE 11. The comparison of the LoS trace between measurement and RT simulation. (a) The evolution of trace parameters vs location. (b) Illustration of the propagation paths within same trace. (c) The comparison of the parameters variation.

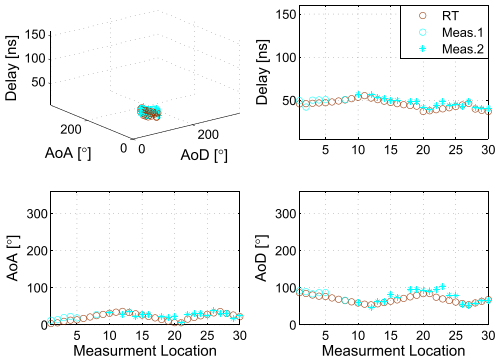

(a)

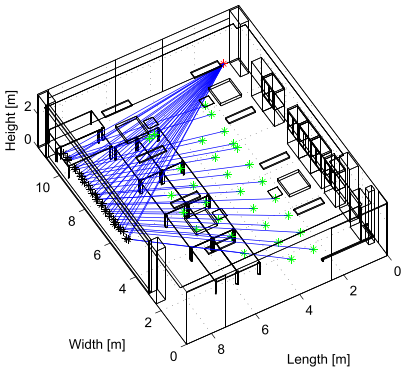

(b)

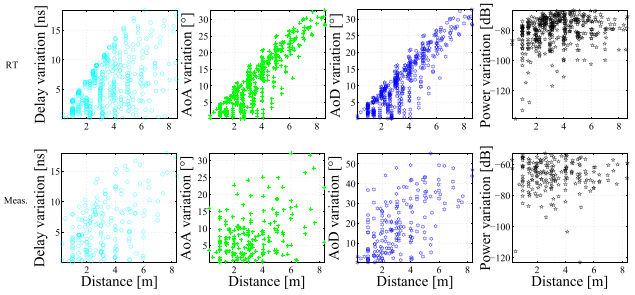

(c)

FIGURE 12. The comparison of the reflection (single bounce) trace between measurement and RT simulation. (a) The evolution of trace parameters vs location. (b) Illustration of the propagation paths within same trace. (c) The comparison of the parameters variation.

general trends of these variations are quite similar for both the measurement-based and the RT simulated results, although the distributions of the parameter variations are more dispersive in the former one. The interdependence among these variations of different parameters, i.e., delay, AoA and power, is evaluated by introducing the cross-correlation coefficient calculated as

$$C = \frac{\sum_{i=1}^{N}(x_i - \bar{X}) \cdot (y_i - \bar{X})}{\sqrt{\sum_{i=1}^{N}(x_i - \bar{X})^2 \cdot \sum_{i=1}^{N}(y_i - \bar{Y})^2}}, \tag{7}$$

where x_i and y_i are the ith element of parameters X and Y, respectively. The $\bar{X}$ and $\bar{Y}$ denote the mean value of samples x_i and y_i, respectively.

According to the results shown in Table 2 and 3, it can be observed that the variations of parameters are highly correlated, especially for the changes of AoAs and AoDs in RT case. The reason is that the detected traces from RT simulations consist of the LoS, single bounce and double bounce paths. The parameters of these paths are geometri-

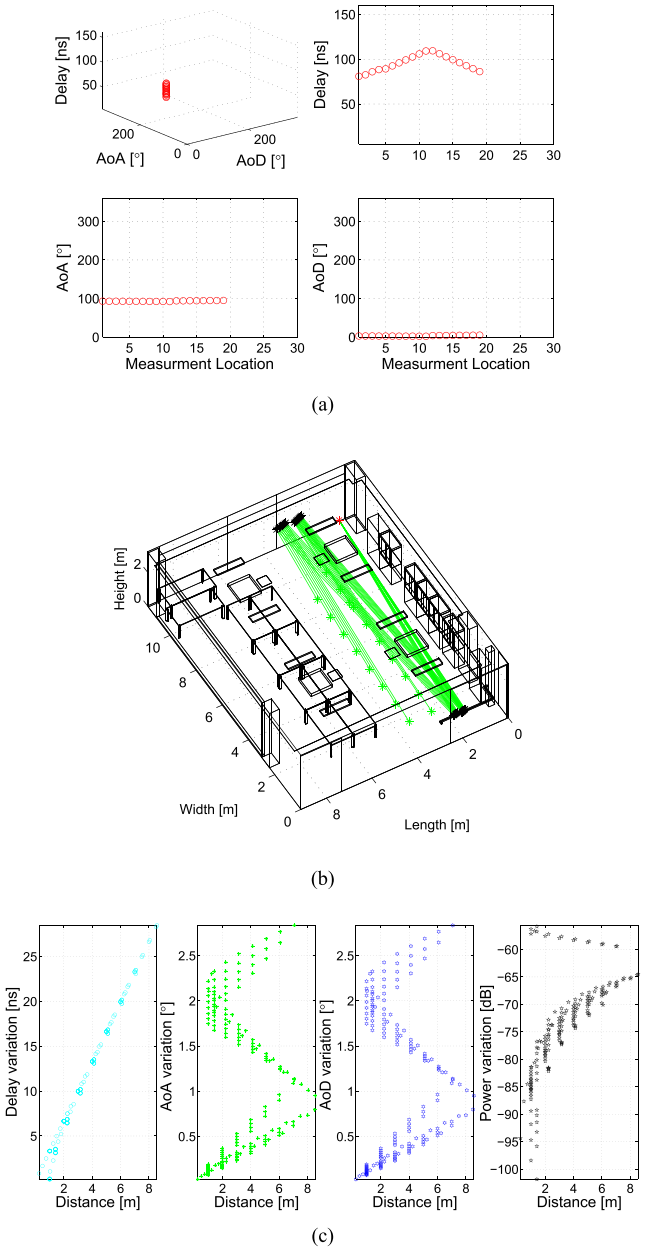

FIGURE 13. The No.1 RT-specified trace. (a) The evolution of trace parameters vs location. (b) Illustration of the propagation paths within same trace. (c) The variations of parameters.

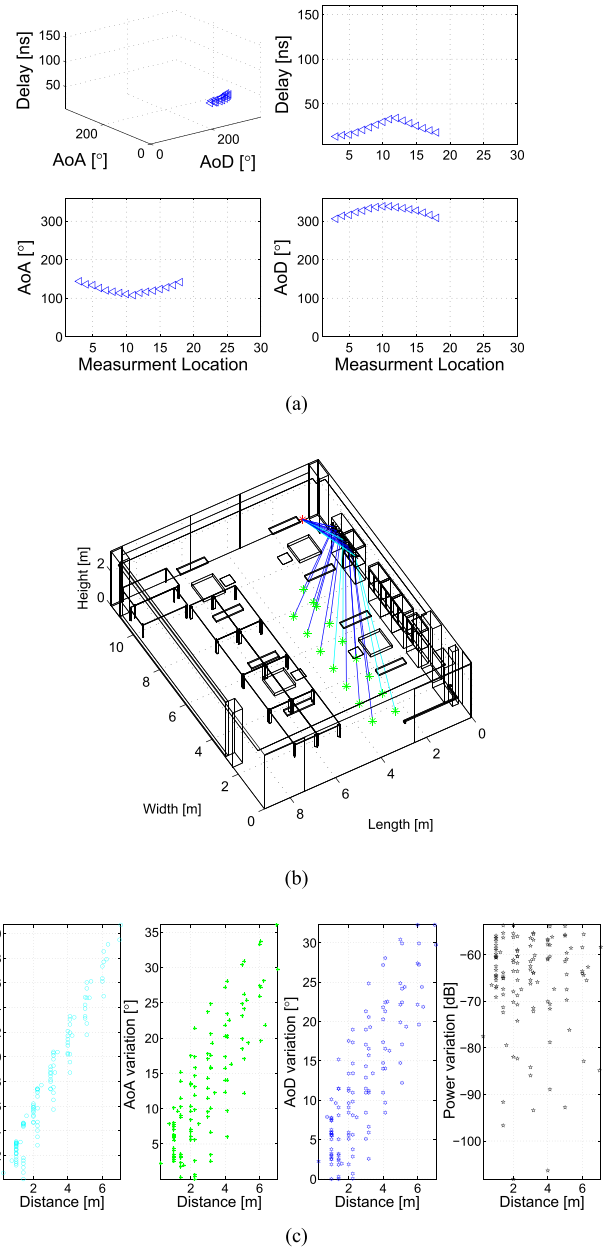

FIGURE 14. The No.2 RT-specified trace. (a) The evolution of trace parameters vs location. (b) Illustration of the propagation paths within same trace. (c) The variations of parameters.

cally calculated, and the variations of these parameters are simultaneous and highly dependent. For the measurement-based results, the continuity of the spatial parameters between two adjacent locations are influenced by the rotation and radiation pattern of the antenna in the measurement. Thus, the correlation between the variations of the AoAs and AoDs decreases.

B. THE ANALYSIS OF THE COMMON TRACES

In order to design and evaluate the performance of beam-related algorithms, such as beam tracking, the behaviors of the traces should also be studied individually. Totally four common traces are identified from the measurement-based and RT simulation results. Two of them, which originate from different propagation mechanisms, are analyzed below.

Figure 11 depicts the LoS traces for both measurement and RT cases. It can be observed that the LoS path obtained from simulation is more stable than the measurement-based result. Larger variations in the spatial domain are experienced at the sharp turning of the UE's movement. The features of single bounce reflected trace are illustrated in figure 12. We can find that two traces from measurement-based results are detected to match the reflected trace obtained from RT simulation as shown in 12(a). It demonstrates that this trace could be divided into several parts because of the missing of channel

samples at some UE's locations during the measurement. Thus, the LDs calculated based on measurement will be shorter than those from the RT and the probability of path's birth-death is correspondingly higher. We also find a common trace originating from the double bounce reflection and it lasts for only four UE's locations.

C. THE ANALYSIS OF RT-SPECIFIED TRACES

In total four traces only existing in the RT results are identified and the analyses of two typical cases are presented. Figure 13 depicts the trace originating from the double reflection and it was observed at 19 UE's locations. We can find that the general trends of the AoA's and AoD's variations are quite similar. It also verifies the rationality of the high cross-correlation between the spatial parameters listed in Table 3. The special trace which consists of paths originating from two different mechanisms is shown in figure 14. It can be found that this trace smoothly varies along UE's movement by involving diffracted path (cyan) and single bounce reflected path (blue) as demonstrated in figure 14(b). By further comparison, we find that the power deviation between these two kinds of paths is non-significant. It demonstrates that the diffracted paths originating from the edges of metal in the indoor environment should still be well considered at high frequencies.

V. CONCLUSIONS

In this paper, the dynamic features of the propagation channel at 23.5 GHz in an indoor conference room have been analyzed. The behaviors of the traces identified from both measurement-based and RT simulation results have been evaluated individually. The proposed "frosted glass" phenomenon, which refers to the influences of current sounding system and antenna radiation pattern, has also been analyzed by further comparisons between the measurement-based and RT simulated channel samples. Results show that the RT-based traces are more stable and survive longer than those from the measurements. It has been found that the LDs of the most traces are within 5 m, which seems to be short but enough for implementing the beam-tracking algorithm by assuming that the normal walking speed of person equals to 1.5 m/s. Moreover, the dominant paths with large power, i.e., LoS and single bounce reflected paths, last much longer. The observation shows that the diffraction is still non-negligible at high frequencies. Meanwhile, high correlations among the parameters' variations within the same trace have been observed. And these variations are limited within certain range.

REFERENCES

[1] *Deliverable D1.1 Scenarios, Requirements and KPIs for 5G Mobile and Wireless System, Mobile and Wireless Communications Enablers for the Twenty-Twenty Information Society (METIS)*, document ICT-317669-METIS/D1.1, METIS, 2014.

[2] T. S. Rappaport *et al.*, "Millimeter wave mobile communications for 5G cellular: It will work!" *IEEE Access*, vol. 1, pp. 335–349, 2013. DOI: 10.1109/ACCESS.2013.2260813

[3] A. Ghosh *et al.*, "Millimeter-wave enhanced local area systems: A high-data-rate approach for future wireless networks," *IEEE J. Sel. Areas Commun.*, vol. 32, no. 6, pp. 1152–1163, Jun. 2014.

[4] S. Sun, T. S. Rappaport, R. W. Heath, A. Nix, and S. Rangan, "MIMO for millimeter-wave wireless communications: Beamforming, spatial multiplexing, or both?" *IEEE Commun. Mag.*, vol. 52, no. 12, pp. 110–121, Dec. 2014.

[5] A. Sayeed and J. Brady, "Beamspace MIMO for high-dimensional multiuser communication at millimeter-wave frequencies," in *Proc. IEEE Global Commun. Conf. (GLOBECOM)*, Dec. 2013, pp. 3679–3684.

[6] J. N. Murdock, E. Ben-Dor, Y. Qiao, J. I. Tamir, and T. S. Rappaport, "A 38 GHz cellular outage study for an urban outdoor campus environment," in *Proc. IEEE Wireless Commun. Netw. Conf. (WCNC)*, Apr. 2012, pp. 3085–3090.

[7] S. Hur, Y.-J. Cho, J. Lee, N.-G. Kang, J. Park, and H. Benn, "Synchronous channel sounder using horn antenna and indoor measurements on 28 GHz," in *Proc. IEEE Int. Black Sea Conf. Commun. Netw. (BlackSeaCom)*, May 2014, pp. 83–87.

[8] S. Hur *et al.*, "Wideband spatial channel model in an urban cellular environments at 28 GHz," in *Proc. 9th Eur. Conf. Antennas Propag. (EuCAP)*, Apr. 2015, pp. 1–5.

[9] J. He, T. Kim, H. Ghauch, K. Liu, and G. Wang, "Millimeter wave MIMO channel tracking systems," in *Proc. Globecom Workshops (GC Wkshps)*, Dec. 2014, pp. 416–421.

[10] V. Degli-Esposti *et al.*, "Ray-tracing-based MM-wave beamforming assessment," *IEEE Access*, vol. 2, pp. 1314–1325, 2014. DOI: 10.1109/ACCESS.2014.2365991

[11] F. Fuschini, E. M. Vitucci, M. Barbiroli, G. Falciasecca, and V. Degli-Esposti, "Ray tracing propagation modeling for future small-cell and indoor applications: A review of current techniques," *Radio Sci.*, vol. 50, no. 6, pp. 469–485, Jun. 2015.

[12] J. J. G. Fernandes, P. F. M. Smulders, and J. C. Neves, "Simulation results on MM-wave indoor radio channel modelling and comparison with measurements," in *Proc. 2nd Symp. Commun. Veh. Technol. Benelux*, Nov. 1994, pp. 89–94.

[13] J. Zhu, H. Wang, and W. Hong, "Large-scale fading characteristics of indoor channel at 45-GHz band," *IEEE Antennas Wireless Propag. Lett.*, vol. 14, pp. 735–738, 2015. DOI: 10.1109/LAWP.2014.2377952

[14] J. Dou *et al.*, "Propagation channel comparison between 23.5 and 45 GHz in conference scenario," *Chin. J. Eng.*, submitted for publication.

[15] H. T. Friis, "A note on a simple transmission formula," *Proc. IRE*, vol. 34, no. 5, pp. 254–256, May 1946.

[16] R. M. A. Azzam and N. M. Bashara, *Ellipsometry and Polarized Light*. Amsterdam, The Netherlands: North Holland, 1987.

[17] R. G. Kouyoumjian and P. H. Pathak, "A uniform geometrical theory of diffraction for an edge in a perfectly conducting surface," *Proc. IEEE*, vol. 62, no. 11, pp. 1448–1461, Nov. 1974.

[18] J. Järveläinen and K. Haneda, "Sixty gigahertz indoor radio wave propagation prediction method based on full scattering model," *Radio Sci.*, vol. 49, no. 4, pp. 293–305, Apr. 2014.

[19] L. Tian, V. Degli-Esposti, E. M. Vitucci, X. Yin, F. Mani, and S. X. Lu, "Semi-deterministic modeling of diffuse scattering component based on propagation graph theory," in *Proc. IEEE 25th Int. Symp. Pers. Indoor Mobile Radio Commun. (PIMRC)*, Sep. 2014, pp. 155–160.

[20] C. Jansen *et al.*, "Diffuse scattering from rough surfaces in THz communication channels," *IEEE Trans. Terahertz Sci. Technol.*, vol. 1, no. 2, pp. 462–472, Nov. 2011.

[21] V. Degli-Esposti, F. Fuschini, E. M. Vitucci, and G. Falciasecca, "Measurement and modelling of scattering from buildings," *IEEE Trans. Antennas Propag.*, vol. 55, no. 1, pp. 143–153, Jan. 2007.

[22] *Propagation Data and Prediction Methods for the Planning of Indoor Radiocommunication Systems and Radio Local Area Networks in the Frequency Range 300 MHz to 100 GHz*, document Rec. ITU-R P.1238-8, 2015.

[23] J. Dou, L. Tian, H. Wang, X. Yuan, N. Zhang, and S. Mei, "45 GHz propagation channel modeling for an indoor conference scenario," in *Proc. IEEE 26th Annu. Int. Symp. Pers., Indoor, Mobile Radio Commun. (PIMRC)*, Apr./Sep. 2015, pp. 2225–2228.

[24] N. Zhang, X. Yin, S. X. Lu, M. Du, and X. Cai, "Measurement-based angular characterization for 72 GHz propagation channels in indoor environments," in *Proc. Globecom Workshops (GC Wkshps)*, Dec. 2014, pp. 370–376.

[25] A. Maltsev *et al.*, "Quasi-deterministic approach to mmWave channel modeling in a non-stationary environment," in *Proc. Globecom Workshops (GC Wkshps)*, Dec. 2014, pp. 966–971.

[26] N. Czink, "The random-cluster model—A stochastic MIMO channel model for broadband wireless communication systems of the 3rd generation and beyond," Ph.D. dissertation, Dept. Electron. Inf. Technol., Vienna Univ. Technol., Vienna, Austria, Dec. 2007.
[27] X. Yin, X. Cai, X. Cheng, J. Chen, and M. Tian, "Empirical geometry-based random-cluster model for high-speed-train channels in UMTS networks," *IEEE Trans. Intell. Transp. Syst.*, vol. 16, no. 5, pp. 2850–2861, Oct. 2015.

NAN ZHANG was born in Qingyang, China, in 1990. He received the bachelor's degree in communication engineering and the master's degree in integrated circuit engineering from Tongji University, Shanghai, China, in 2012 and 2015, respectively.

He is currently a Senior Engineer with the Department of Algorithms, ZTE Corporation. His current research interests are in the field of 5G channel modeling and new air-interface.

JIANWU DOU was born in Yuci, China, in 1973. He received the Ph.D. degree in robotic mechanism from the Beijing University of Technology, Beijing, China, in 2001. From 2000 to 2014, he was the Head of the wireless RRM team, including 2G/3G/4G/WLAN, and was in charge of developing multi-RAT wireless system simulation platform. From 2012 to 2014, he was also the Product Manager of ZTE iNES, a multi-cell/multi-UE hardware wireless channel emulator.

He is currently in charge of a National Science and Technology Major Project of the Ministry of Science and Technology of China and participated in the 5G project sponsored by the National Natural Science Foundation of China. He is the Vice Director of the Department of Algorithms with ZTE Corporation. His current research interests are in the field of 5G channel modeling, new air-interface, and high-layer design.

Dr. Dou achieved the Science and Technology Award (First Level) from the China Institute of Communications in 2014 and the Award for Chinese Outstanding Patented Invention from WIPO-SIPO in 2011.

LI TIAN was born in Xiantao, China, in 1988. He received the bachelor's degree in communication engineering and the Ph.D. degree in control science and control engineering from Tongji University, Shanghai, China, in 2009 and 2015, respectively. From 2013 to 2014, he was a Visiting Ph.D. Student with the Department of Electronics and Information Systems, University of Bologna, working with Prof. V. Degli-Esposti.

He participated in the 5G project sponsored by the National Natural Science Foundation of China. He is currently a Senior Engineer with the Department of Algorithms, ZTE Corporation. His current research interests are in the field of 5G channel modeling and new air-interface.

Dr. Tian serves as a Reviewer for a number of international journals, including the IEEE Transactions on Vehicular Technology, the IEEE Access, the IEEE Antennas and Wireless Propagation Letters, and the *International Journal of Antennas and Propagation*.

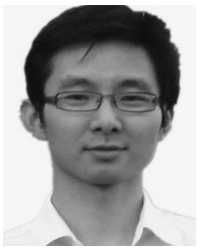

XI YUAN was born in Jiangxi, China, in 1984. He received the master's degree in communication and information system from Harbin Engineering University, in 2009. He was a member of the wireless system simulation team, involved in 2G/3G/4G research, and was in charge of developing ray tracing simulation platform. He has engaged in communication system simulation researching since joining ZTE Corporation. His current research interests are in the field of 5G channel modeling and new air-interface.

XIAOYI YANG was born in Qiqihaer, China, in 1978. He received the master's degree in communication and information system from Northeastern University, in 2008. He has engaged in communication system simulation researching since joining ZTE Corporation. His work involved in 2G/3G/4G system, and is a member of the ZTE 5G high frequency team.

SUPING MEI was born in Hangzhou, China, in 1984. She received the master's degree in communication and information systems from Tongji University, Shanghai, China, in 2010. She joined ZTE Corporation in 2010. She is currently a Simulation System Engineer with the Department of Algorithms, Wireless Product Operation. Her current research interests including 5G channel modeling and channel measured data analyzing.

HAIMING WANG was born in Jiangyin, China, in 1975. He received the M.S. and Ph.D. degrees in electrical engineering from Southeast University, Nanjing, China, in 2002 and 2009, respectively. He joined the State Key Laboratory of Millimeter Waves, Southeast University, in 2002, where he is currently an Associate Professor. His current research interests include signal processing for wireless communications and millimeter-wave wireless communications. He received the first-class Science and Technology Progress Award of Jiangsu Province of China in 2009. He serves as the Vice Chair of the IEEE 802.11aj Task Group. He also serves as a Reviewer for a number of international journals, including the IEEE Transactions on Communications, the IEEE Transactions on Wireless Communications, the IEEE Transactions on Vehicular Technology, the IEEE Transactions on Instrumentation and Measurement, the IEEE Communications Letters, and the IEEE Signal Processing Letters.